Polymorphous Packing of Pentagonal Nanoprisms

Jules Marcone, Wajdi Chaâbani, Claire Goldmann, Marianne Impéror-Clerc, Doru Constantin, Cyrille Hamon

Polymorphous packing of pentagonal nanoprisms

Jules Marcone,[†] Wajdi Chaâbani,[†] Claire Goldmann,[†] Marianne Impéror-Clerc,[†] Doru Constantin,[*,‡] and Cyrille Hamon[*,†]

[†]*Laboratoire de Physique des Solides, CNRS and Université Paris-Saclay, 91400 Orsay, France*

[‡]*Institut Charles Sadron, CNRS and Université de Strasbourg, 67034 Strasbourg, France*

E-mail: constantin@unistra.fr; cyrille.hamon@universite-paris-saclay.fr

Abstract

Packing solid shapes into regular lattices can yield very complex assemblies, not all of which achieve the highest packing fraction. In two dimensions, the regular pentagon is paradigmatic, being the simplest shape that does not pave the plane completely. In this work, we demonstrate the packing of plasmonic nanoprisms with pentagonal cross section, which form extended supercrystals. We do encounter the long-predicted ice-ray and Dürer packings (with packing fractions of 0.921 and 0.854, respectively), but also a variety of novel polymorphs that can be obtained from these two configurations by a continuous sliding transformation and exhibit an intermediate packing fraction. Beyond the fundamental interest of this result, fine control over the density and symmetry of such plasmonic assemblies opens the perspective of tuning their optical properties, with potential applications in metamaterial fabrication, catalysis or molecular detection.

Keywords

nanoparticles, pentagonal packing, silver nanorods, superlattices, self-assembly

Covering the plane with regular shapes is a complex and intriguing question that has seen sustained interest since antiquity. Among these shapes, regular pentagons are special because unlike triangles, squares and hexagons, they do not tile the plane without gaps. This made them attractive for use in decorative patterns, such as the traditional Chinese ice-ray motif inspired by the growth of ice crystals into 'rays',[1] which is a periodic striped phase consisting of alternate rows of pentagons in two different orientations. European scientists, philosophers and artists, such as Albrecht Dürer[2] or Johannes Kepler,[3] also studied regular arrangements of pentagons, like the so-called Dürer packing. Hales and Kusner have recently demonstrated by a computer-assisted proof[4] that the ice-ray configuration has the largest possible packing fraction η defined as the ratio of the area covered by the objects to the total area ($\eta = 0.921$). Ice-ray packing was first demonstrated in numerical simulations in 2005, by the group of Frenkel.[5] At lower packing fraction a rotator/plastic phase was found, in which the orientational order for the pentagons was lost while the positional order adopted a hexagonal arrangement. Mathematicians have predicted the existence of other crystalline polymorphs with a slightly lower packing fraction,[4,6–8] but these lattice polymorphs have yet to be encountered in experiments.

The first experiments about pentagonal packing were done at the macroscopic scale, on an air table, and provided insight into such arrangements.[9,10] More recently, micron-sized pentagonal polymeric platelets were fabricated and assembled into colloidal monolayers: they exhibited a rotator phase, but no crystalline structures.[11] At the molecular length scale, a few examples of pentagonal clusters assembled on a substrate have been demonstrated.[12–15] Finally, at the atomic length scale, phosphorus pentamers deposited on a Ag(111) substrate can pack into a dense monolayer, consisting of alternate rows of pentagons in two different orientations, resembling the ice-ray arrangement.[16]

Considering the imaging difficulties at the atomic scale and the equilibration issues at the macroscale, a promising alternative for obtaining pentagonal packing is the use of nano-objects. In this respect, metallic nanoparticles are excellent candidates due to their

monodispersity, large size compared to molecules and high electron density. For instance, we have recently obtained three-dimensional supercrystals (SCs) of truncated pentatwinned gold bipyramids that show a double-lattice packing related to the pentagonal ice-ray.[17] Pentatwinned anisotropic metallic nanoparticles have been assembled into standing monolayers on a substrate,[18,19] but so far only plastic crystals[20] or an apparent hexagonal order[21] have been reported. The discrepancy with the predictions above might be due to a large polydispersity in terms of size and shape or to their small width, which renders difficult the identification of the pentagonal cross section with a scanning electron microscope (SEM). We therefore hypothesized that noble metal nanoprisms (NPs) with a large enough regular pentagonal cross-section and low size dispersity would be ideal building blocks to observe 2D pentagonal packing.

Here we show that monodisperse pentatwinned gold/silver NPs assemble spontaneously into extended SCs with a characteristic trapezoidal shape. Careful analysis of the intralayer organization reveals that the NPs pack into very regular structures, mostly corresponding to the pentagonal ice-ray. Other less dense crystalline polymorphs are often observed, including the Dürer packing as well as intermediate configurations obtained via a continuous sliding transformation.[4]

The experimental system consists in elongated pentagonal silver NPs prepared from gold decahedron seeds,[22] which have a nearly constant length of about 140 nm and a width spanning from 27.5 to 81.7 nm. Byproducts corresponding to triangular right bipyramids, spheroids, and cubes were discarded by selective precipitation of the nanoprisms via depletion-induced self-assembly.[23] This step is important, as the presence of byproducts would otherwise affect the extension of the NP layers. Similar SCs were obtained for all NPs with different widths, showing an increasing orientational ordering for the larger NPs (see Section 2 in the Supporting Information for a complete discussion about the optimization of the self-assembly conditions).[24–29] In the following, we present the results for only one width, for gold/silver NPs of 143.7 ± 9.2 nm in length and 74.8 ± 3.2 nm in width. Scanning

electron microscopy (SEM) images show that, after drying on a Si wafer, the NPs solutions leave behind micron-sized SCs with a trapezoidal shape (Figure 1(a-b)). At higher magnification, a multi-layered structure of closely packed nanoprisms in a standing orientation is observed (Figure 1(c-d) and Section 3 in the Supporting Information). The shape of these SCs is different from that usually expected for a SC of standing nanorods in a hexagonal arrangement, which tend to adopt a circular or hexagonal macroscopic shape.[19,30] Since the SC shape can be related to the local arrangement of the NPs, the obtention of SCs with a trapezoidal shape is a first indication of a new lattice structure. Close view of the SC reveals the pentagonal section of the nanoprisms, often arranged in alternating stripes in an ice-ray fashion. The trapezoidal shape of the SCs can be recovered by combining three Delaunay triangles of the ice-ray unit cell (Figure 1b, f). To assess the symmetry of the lattice inside the SCs, fast Fourier Transforms (FFT) were performed on the SEM experimental images and on model images for comparison (see Figure 2). Although the FFTs are close to a hexagonal pattern, the spots are not arranged along a regular hexagon, and they display the $\mathbf{a}^*$ (10) and $\mathbf{b}^*$ (01) spots characteristic of the ice-ray packing with a rectangular symmetry (see Figure 2(a-b)). FFT analysis on a large SC area (see Section 2 in the Supporting Information) confirms the extension of the ice-ray packing to tens of micrometers (i.e. the SC size). In order to confirm that the rectangular symmetry is linked to the pentagonal cross-section, we conducted the self-assembly of monocrystalline gold nanorods for comparison. In this case, the nanorods are arranged in an hexagonal lattice, as confirmed by the FFT and the corresponding model images (Figure 2(c-d)). Such hexagonal ordering has already been reported for monocrystalline nanorods having an octogonal cross section, which is very close to a circular one.[18,19,21,30,31] Taken together, this set of experiments shows that the rectangular lattice arises from the asymmetric cross section of the pentagonal nanorods, resulting in lower symmetry of the nanostructure.

We next performed SEM image analysis in order to quantify the orientation distribution of the pentagonal cross-section of the NPs within the SCs. Particle outlines were extracted

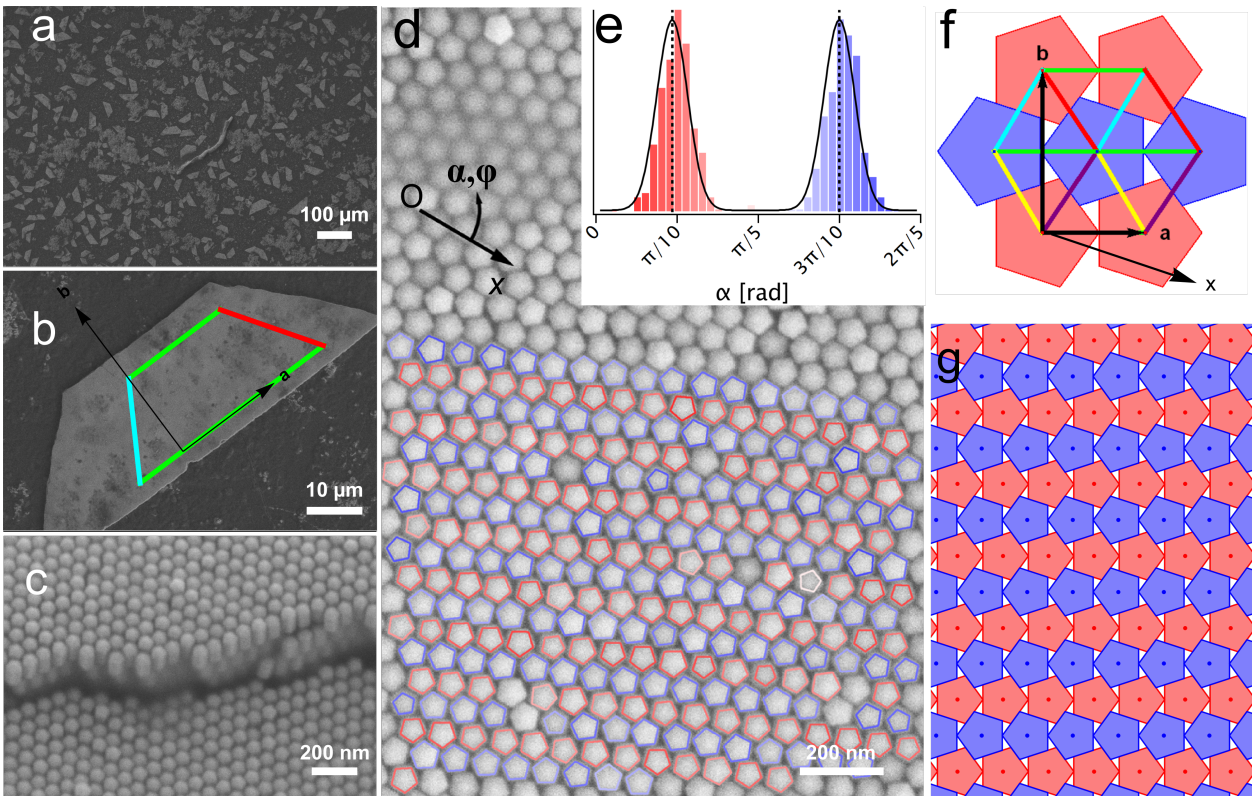

Figure 1: Supercrystals with ice-ray packing. (a-b) SEM images of trapezoidal SCs at different magnifications. (c) Side view showing the 2D packing of the nanoprisms at the surface of the SCs. (d) Close view of an SC surface. The pentagonal cross-section of the NPs is visible in the SEM image. Pentagonal contours are overlaid in the bottom half, color coded to the particles' orientation with respect to the Ox axis, shown as black arrow. (e) Histogram of the orientation angle α for the pentagonal cross-section in (d), with the same color code, and Gaussian fits (solid line). (f) Ice-ray packing annotated with color-coded Delaunay triangles (each color stands for one distance) as well as vectors **a** and **b** of the rectangular unit cell. (g) 2D ice-ray packing of regular pentagons. The blue and red colors indicate the two pentagon orientations.

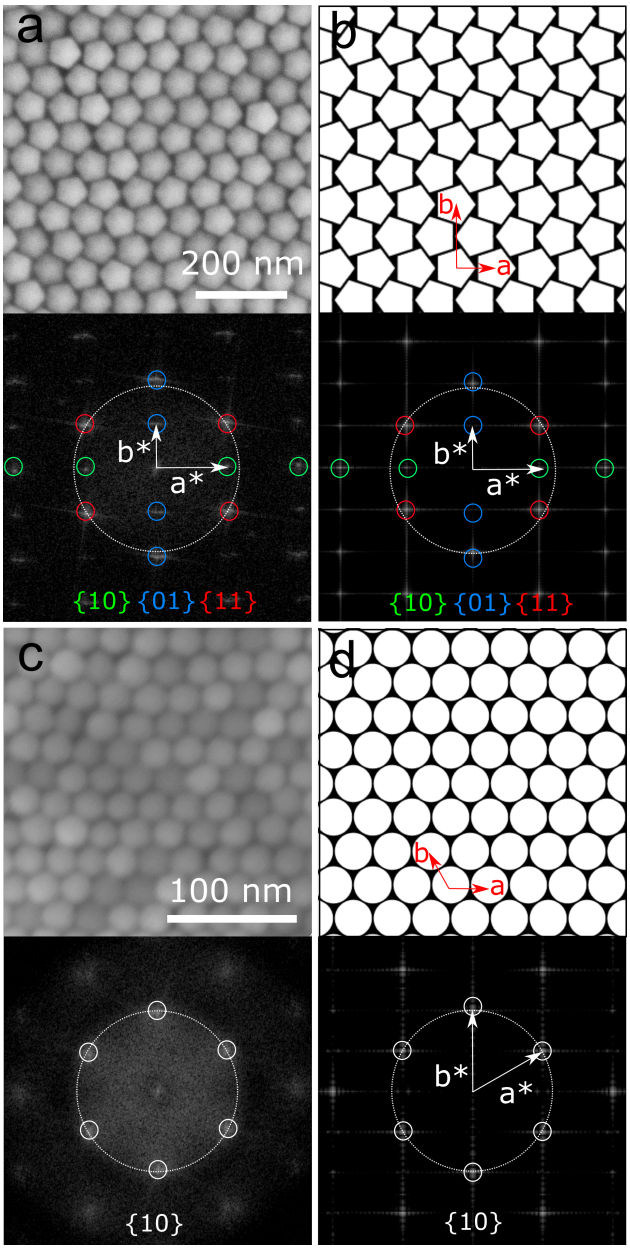

Figure 2: Rectangular versus hexagonal crystalline order. (a) top) SEM image of a rectangular lattice of standing pentagonal gold/silver nanoprisms. bottom) corresponding FFT image (b) top) model of a rectangular lattice of regular pentagons (ice-ray packing). bottom) corresponding FFT image (c) SEM image of a hexagonal lattice of standing monocrystalline gold rods. bottom) corresponding FFT image (d) top) model of a hexagonal lattice of disks. bottom) corresponding FFT image.

from the SEM images and fitted with regular pentagons (Figure 1d) and Section 2 in the Supporting Information). Their orientation is defined by an angle $\alpha \in [0, 2\pi/5]$ with respect to an in-plane Ox axis. The local packing structure is shown in Figure 1f and the analysis of the orientation angle α for Figure 1d is given in panel (e). The entire field of view consists of stripes of particles with two alternate orientations, distinguished by the red or blue outline color. The bimodal orientation histogram is well described by the sum of two Gaussian peaks of equal height and width, with a peak spacing within 0.02 rad of the theoretical $\pi/5$ rad value. Along with the rectangular lattice symmetry, this bimodal orientation distribution proves the formation of the ice-ray packing, with two orientations for the pentagons related by a $\pi/5$ rotation.

As discussed above, the ice-ray packing is not the only possible one: the Dürer packing is also a potential candidate. We do encounter it in the SCs, as shown by the SEM image in Figure 3(b), where a grain boundary separates an ice-ray domain (on the left) from a Dürer one (on the right), easily identifiable by the parallel stripes of pentagon dimers. Both the boundary and the row limits are marked by white dashed lines. For comparison, the image is flanked by pictures of the ideal ice-ray and Dürer packings (in panels (a) and (c), respectively.) Panel (d) shows the orientation distributions in the two domains (Dürer on top and ice-ray at the bottom), obtained as in Figure 1(e). The half-width of the peaks differs significantly between the ice-ray (0.04 ± 0.002 rad) and the Dürer (0.05 ± 0.004 rad.) domains, indicating lower orientational order in the latter. Note that, in the Dürer phase, we subtracted from the α values a systematic drift from left to right of the image, so that the given half-width only corresponds to local orientation fluctuations.

The ice-ray and the Dürer packings are linked to each other by a simple geometrical transformation.[4,7] Let us return to the rectangular unit cell of the ice-ray packing: it contains two pentagons in two different orientations, depicted in red and blue (Figure 1(f)). These two adjacent pentagons can slide along their common edge, resulting in a shift of the position of the inversion center (see Figure 3(e)). This local motion is the starting point of a global

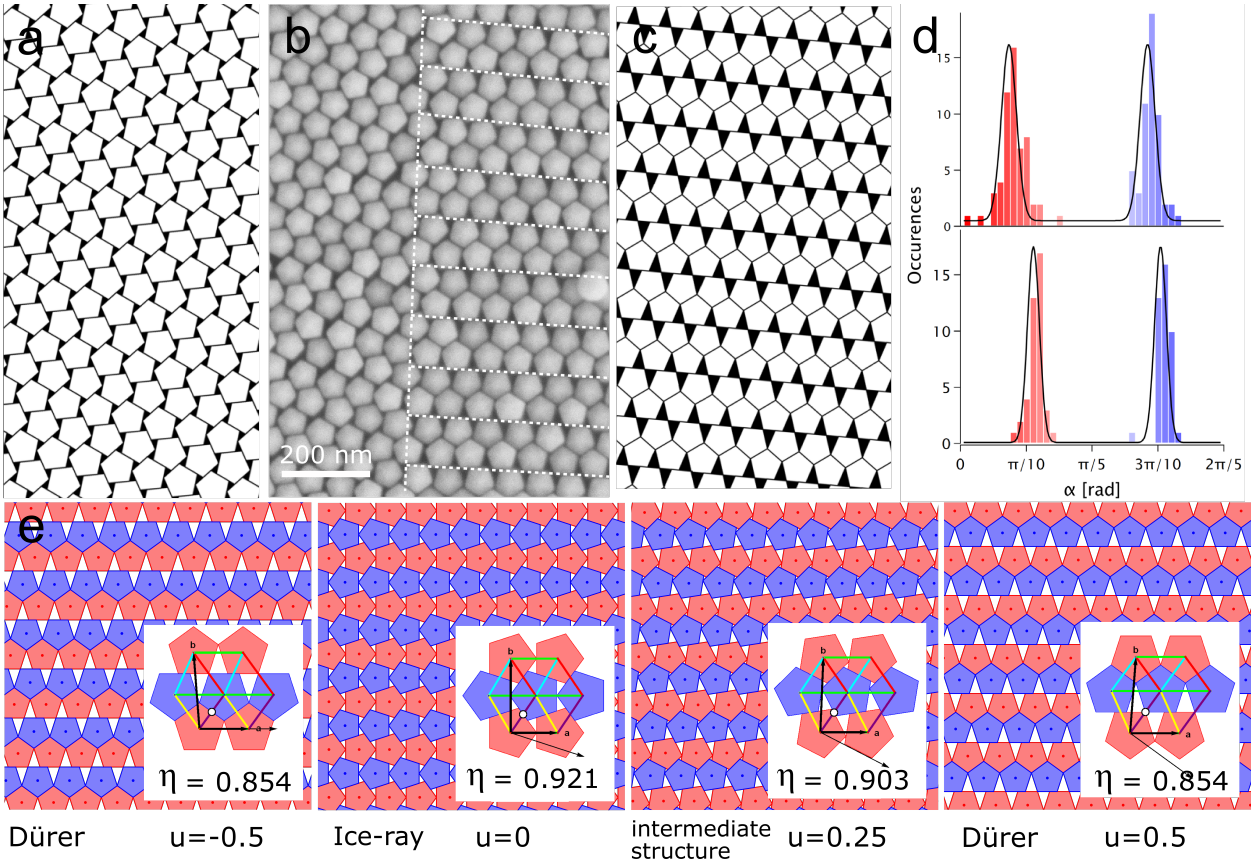

Figure 3: Grain boundary between ice-ray and Dürer domains. (a) Ideal ice-ray packing. (b) SEM image of an SC surface showing both ice-ray (on the left) and Dürer (on the right) arrangements. The boundary is marked by a dashed white line, as are the limits of the dimer rows in the Dürer domain. (c) Ideal Dürer packing. (d) Histogram of the particle orientation α in the Dürer (top) and ice-ray (bottom) domains, with Gaussian fits. (e) Scheme of the continuous sliding deformation from the ice-ray to the Dürer packing. Values of the corresponding sliding parameter u and packing fraction η are given. The position of the inversion center is depicted by a white circle and slides along the common edge of the blue and red pentagons. Note the deformation of the unit cell from rectangular to oblique and the tilt in orientation of the pentagons with respect to the stripe direction along **a**. The thin black arrow indicates the direction of the Ox axis used as angle reference for the image analysis (see Figures 1, 3, 4).

sliding transformation of the whole packing. As a result, a continuous family of crystalline polymorphs is obtained, all having a slightly lower packing density than the ice-ray packing. Note that the relative angle of $\pi/5$ between the two orientations for pentagons is preserved upon sliding. Calculations are detailed in Section 3 in the Supporting Information, introducing a sliding parameter u that corresponds to the shift of the inversion center along the edge. This sliding transformation leads continuously from the ice-ray packing ($u = 0$, $\eta = 0.921$) to a Dürer packing ($u = 0.5$, $\eta = 0.854$) (see Figure 3(e)).[4] Doing so, the alternate rows in two different orientations slide along each other and the pentagons tilt with respect to the row direction. Sliding induces the unit cell $(\mathbf{a}, \mathbf{b})$ to become oblique instead of rectangular and the space group changes from pm to $p2$ when u is different from zero.

The arrangements we observe experimentally indeed reside along the continuum between the ideal ice-ray and Dürer packings, as shown by the analysis of the SEM image in Figure 4, corresponding to a polymorph with an intermediate sliding deformation ($u = 0.1$, $\eta = 0.918$). We first determine by image analysis both the distribution for the orientation of the pentagons (angle α in Figure 4(b,c)) and for the bonds between the centers of neighboring particles (angle ϕ in Figure 4(d,e)). Five different orientations of bonds are found and are plotted in different colors. We plot the bond length vs. orientation in Figure 4(e) and compare it to the predictions of the sliding transformation (see Section 4 in the Supporting Information) for the two limiting cases ($u = 0$ and $u = 0.5$) and for the configuration with $u = 0.1$ that best fits the data shown in Figure 4(a). This polymorph is close to the ice-ray but definitely different, with a unit cell that is not rectangular but oblique.

Finally, crystal twinning between domains is also encountered as illustrated in Figure 5. The SEM image shows an area where two domains are separated by a twinning line shown as a white dashed line. These domains correspond to two twin crystals of the ice-ray packing (Figure 5(a)), in which the twinning line is oriented along $(\mathbf{a} + \mathbf{b})$ and $(\mathbf{a} - \mathbf{b})$ respectively. Rows of particles with the same orientation have a kink at the boundary line (close to a $\pi/3$ angle), resulting in a herringbone texture (Figure 5(b)). Remarkably, the two pentagon

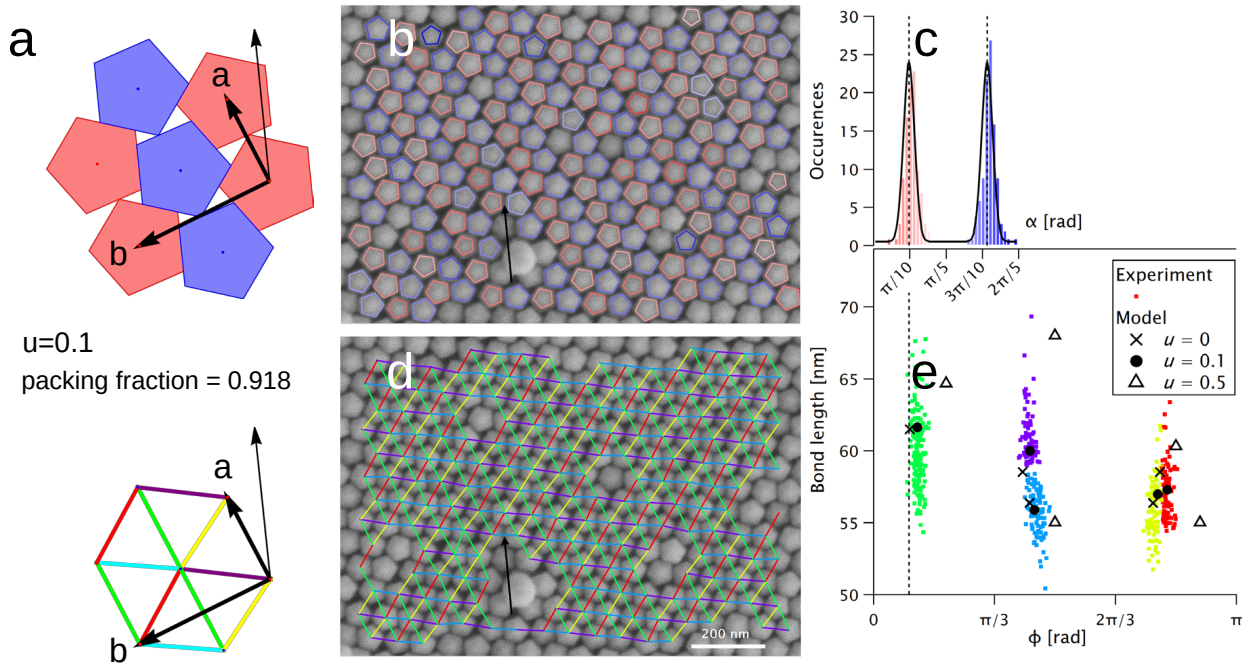

Figure 4: Analysis of orientational and translational order in a lattice polymorph. (a) Scheme of the polymorph with a sliding parameter of $u = 0.1$ and a packing fraction of 0.918. The unit cell is oblique. The thin black arrow corresponds to the Ox axis, common reference for the α and ϕ angles. (b) SEM image with overlaid particle contours. (c) Histogram of the particle orientations (angle α). (d) The bonds between the centers of neighboring particles are shown by overlaid links, color coded by length and orientation (angle ϕ). (e) Plot of the bond length vs. bond orientation. Colored points correspond to the experimental image with the same color code as in (d). Symbols are the predictions for the length and orientation of the five different bonds: ice ray-lattice ($u = 0$, crosses), Dürer lattice ($u = 0.5$, triangles) and the intermediate value ($u = 0.1$ solid dots) that best approaches the experimental data points.

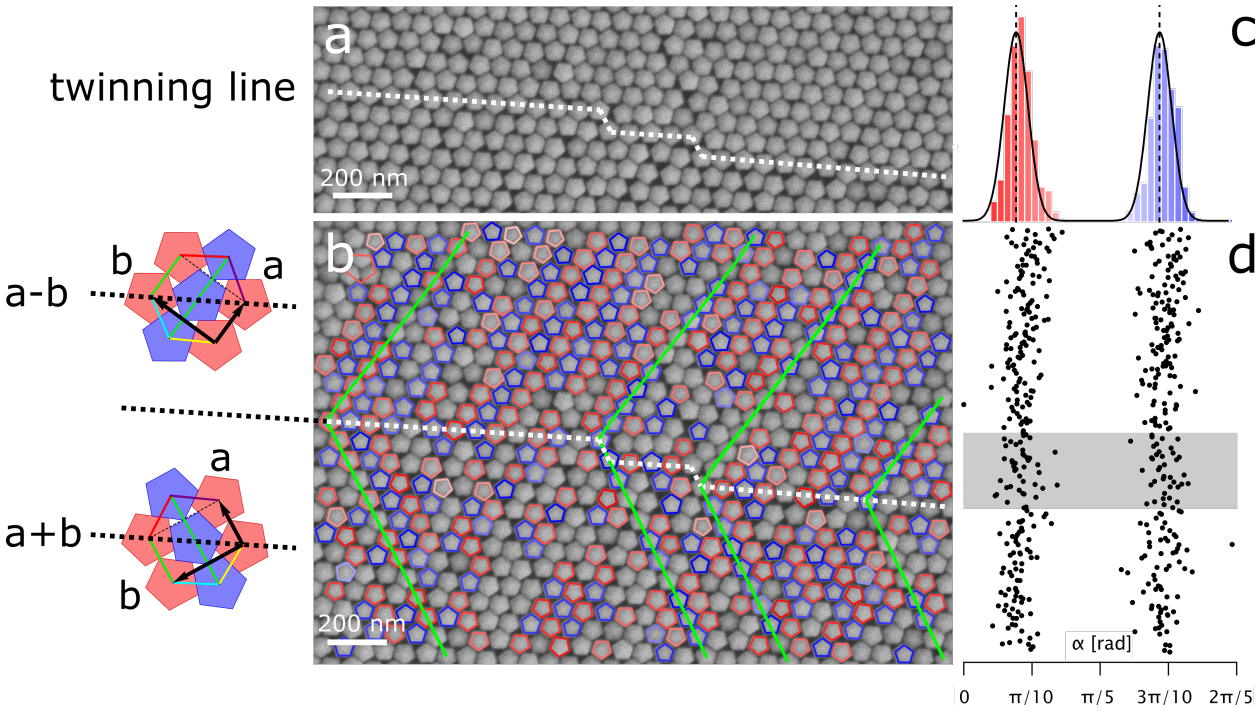

Figure 5: Twinning line between two domains forming a herringbone texture. (a) SEM image of a defect highlighted with a dashed white line corresponding to a twinning line. (b) Same image where the pentagonal contours are overlaid, color coded to the particles' orientation. The green lines are plotted manually along some pentagon rows to highlight the herringbone texture. On the left, the scheme of the unit cell is shown for each crystal. (c) Histogram of the particle orientations and (d) corresponding height-resolved plot of the orientation. The grey overlay indicates the area covered by the twinning line.

orientations (marked as red and blue) are conserved across the twinning line, as shown by the height-resolved plot of the orientation α and the associated histogram (Figure 5(c,d)). Indeed, on the SEM image without the orientation overlay (Figure 5(a)), the twinning line is indiscernible by eye. In contrast to other superlattices,[26,32,33] such as rhombic platelet lattices,[33] we find that crystal twinning in pentagonal SCs only induces positional disorder while the orientational order is preserved.

So far, only a few examples of the ice-ray pentagonal packing had been encountered, either at the macroscale or at the molecular/atomic scale. Here we obtain a first experimental realisation at the mesoscale with silver nanoprisms self-assembled into extended micron-sized supercrystals (Figure 1). In contrast with plastic/rotator phases, the NPs display high positional and orientational ordering related by a $\pi/5$ rotation. Extended crystalline order is present and its symmetry is not hexagonal but rectangular, which is a clear signature of the ice-ray pentagonal packing, as proven by the Fourier transform images (Figure 2). The trapezoidal shape of the SCs is related to the symmetry of the unit cell (via its Delaunay triangles), confirming both the very long-range order of the lattices (extending over hundreds of particle rows) and, indirectly, the excellent size and shape monodispersity of the samples. The presence of polymorphs for crystalline pentagonal packing gives rise to a rich phase behavior. Along with the ice-ray packing, other crystalline structured are evidenced, like the Dürer packing (Figure 3) and intermediate polymorphs (Figure 4). Crystal twinning is also observed (Figure 5). A sliding transformation is introduced to explain such polymorphism (Figure 3(e)). Our analysis reveals a subtle interplay between orientational and positional order. On the one hand, pentagon orientation is conserved even across the boundary between two twin ice-ray crystals or between two types of packing (e.g. ice-ray and Dürer). On the other hand, as the particle's width gets smaller, orientational order decreases while the positional one, given by the length and orientation of the bonds between neighboring NPs, remains fairly constant. Thus, the lattice persists even as the disorientation increases, supporting the presence of the rotator phase detected in numerical simulations.[5]

The presence of polymorphs can be rationalized by a compromise between the structure that reaches the densest packing (i.e. ice-ray) and the structure that maximizes face to face contact (i.e. Dürer). Although the Dürer structure is less dense than the ice-ray, it allows the formation of face-to-face interparticle contacts, which are favored by strong and localized interactions such as the Van der Waals attraction. This results in the formation of many lattice polymorphs that can be described by the continuous sliding transformation between the two structures. In this sense, the nanoprisms we study in this work are different from other polyhedral nanocrystals such as octahedra, which assemble in a few discrete lattice polymorphs.[26,34–36]

Compared to earlier macroscopic assemblies[9] and numerical simulation studies of hard pentagons,[37,38] such supercrystals display a rich phase diagram and open the way to further studies. For instance, in depth investigation of the self-assembly kinetics may reveal the trajectories of materials formation. Varying experimental conditions should help addressing the open and general question of the relative stability of different lattice polymorphs. As pointed out recently,[39] minimising the packing fraction is not the only parameter relevant for hard colloid crystallization. In this respect, packing pentagonal nanoprisms appears as a promising model system to study crystallization at the mesoscale. The Dürer packing is promising for material design due to the formation of nanochannels between the NPs that would enhance molecular diffusion. Note that an infinity of Dürer tilings exist (with the same packing fraction), but we only observed the one obtained by sliding from the ice-ray configuration. However, a version where all pentagons are in the edge-to-edge configuration would have twice the nanochannel cross-section compared to the Dürer lattices described in this work. Numerical simulations (see the supplementary videos) show that the electric field distribution is different for the various lattice polymorphs, a result that is relevant for plasmon-enhanced spectroscopy and that opens the perspective of using these assemblies for the development of sensing applications.

Acknowledgement

The CNRS is acknowledged for funding and support. This work has benefited from an Investissements d'Avenir grant from Labex PALM (ANR-10-LABX-0039-PALM). J. M. acknowledges financial support by the ANR NIMROD project (ANR-21-CE09-0019) for his PhD. The present work has benefited from the electronic microscopy facility of Imagerie-Gif, (http://www.i2bc.parissaclay.fr), member of IBiSA (http://www.ibisa.net), supported by "France-BioImaging" (ANR10-INBS-04-01), and the Labex "Saclay Plant Science" (ANR-11-IDEX-0003-02). We thank Frederic Kanoufi, Jean-Yves Piquemal and Miguel Comesaña-Hermo for help with the numerical simulations.

Supporting Information Available

Synthesis and purification protocols, characterization of the nanoparticles, additional SEM images, image analysis and geometrical relations are available on-line. Numerical simulations showing that the electric field distribution is different for the various lattice polymorphs are provided as four supplementary videos. The Mathematica notebook used to model the sliding transformation is available at:

`https://www.wolframcloud.com/obj/c70ae9fa-d6a8-4061-9fad-69d93cd42ccf`

References

(1) Dye, D. S. *A Grammar of Chinese Lattice*; SMC Pub. Inc: Taipei, 1949.

(2) Dürer, A. *Underweysung der Messung, mit dem Zirckel und Richtscheyt, in Linien, Ebenen unnd gantzen corporen*; Hieronymus Andreae, Nüremberg, Germany, 1525; p 62, `https://de.wikisource.org/wiki/Underweysung_der_Messung,_mit_dem_Zirckel_und_Richtscheyt,_in_Linien,_Ebenen_unnd_gantzen_corporen`.

(3) Kepler, J. *Harmonices Mundi*; Gottfried Tambach, Linz, Austria, 1619; pp 1–255, http://archive.org/details/ioanniskepplerih00kepl.

(4) Hales, T.; Kusner, W. Packings of Regular Pentagons in the Plane. arXiv (Mathematics, Metric Geometry), 2016; DOI: 10.48550/arXiv.1602.07220 (accessed March 13, 2021).

(5) Schilling, T.; Pronk, S.; Mulder, B.; Frenkel, D. Monte Carlo Study of Hard Pentagons. *Phys. Rev. E* **2005**, *71*, 036138.

(6) Henley, C. L. Sphere Packings and Local Environments in Penrose Tilings. *Phys. Rev. B* **1986**, *34*, 797–816.

(7) Kuperberg, G.; Kuperberg, W. Double-Lattice Packings of Convex Bodies in the Plane. *Discrete & Computational Geometry* **1990**, *5*, 389–397.

(8) Quiquandon, M.; Gratias, D.; Sirindil, A.; Portier, R. Merohedral twins revisited: quinary twins and beyond. *Acta Crystallogr A Found Adv* **2016**, *72*, 55–61.

(9) Duparcmeur, Y. L.; Gervois, A.; Troadec, J. P. Dense Periodic Packings of Regular Polygons. *J. Phys. I* **1995**, *5*, 1539–1550.

(10) Duparcmeur, Y. L.; Gervois, A.; Troadec, J. P. Crystallization of Pentagon Packings. *J. Phys.: Condens. Matter* **1995**, *7*, 3421–3430.

(11) Zhao, K.; Mason, T. G. Frustrated Rotator Crystals and Glasses of Brownian Pentagons. *Phys. Rev. Lett.* **2009**, *103*, 208302.

(12) Bauert, T.; Merz, L.; Bandera, D.; Parschau, M.; Siegel, J. S.; Ernst, K.-H. Building 2D Crystals from 5-Fold-Symmetric Molecules. *J. Am. Chem. Soc.* **2009**, *131*, 3460–3461.

(13) Ren, C.; Zhou, F.; Qin, B.; Ye, R.; Shen, S.; Su, H.; Zeng, H. Crystallographic Realization of the Mathematically Predicted Densest All-Pentagon Packing Lattice by C5-Symmetric "Sticky" Fluoropentamers. *Angew. Chem. Int. Ed.* **2011**, *50*, 10612–10615.

(14) Yuan, C.; Xue, N.; Zhang, X.; Zhang, Y.; Li, N.; Xue, Q.; Wu, T.; Hou, S.; Wang, Y. A Two-Dimensional Crystal Formed by Pentamers on Au(111). *Chem. Commun.* **2019**, *55*, 5427–5430.

(15) Wasio, N. A.; Quardokus, R. C.; Forrest, R. P.; Lent, C. S.; Corcelli, S. A.; Christie, J. A.; Henderson, K. W.; Kandel, S. A. Self-assembly of hydrogen-bonded two-dimensional quasicrystals. *Nature* **2014**, *507*, 86–89.

(16) Zhang, W.; Enriquez, H.; Tong, Y.; Mayne, A. J.; Bendounan, A.; Dappe, Y. J.; Kara, A.; Dujardin, G.; Oughaddou, H. Phosphorus Pentamers: Floating Nanoflowers Form a 2D Network. *Adv. Funct. Mater.* **2020**, *30*, 2004531.

(17) Lyu, J.; Chaâbani, W.; Modin, E.; Chuvilin, A.; Bizien, T.; Smallenburg, F.; Impéror-Clerc, M.; Constantin, D.; Hamon, C. Double-Lattice Packing of Pentagonal Gold Bipyramids in Supercrystals with Triclinic Symmetry. *Adv. Mater.* **2022**, *34*, 2200883.

(18) Guerrero-Martínez, A.; Pérez-Juste, J.; Carbó-Argibay, E.; Tardajos, G.; Liz-Marzán, L. M. Gemini-Surfactant-Directed Self-Assembly of Monodisperse Gold Nanorods into Standing Superlattices. *Angew. Chem. Int. Ed.* **2009**, *48*, 9484–9488.

(19) Scarabelli, L.; Hamon, C.; Liz-Marzán, L. M. Design and Fabrication of Plasmonic Nanomaterials Based on Gold Nanorod Supercrystals. *Chem. Mater.* **2017**, *29*, 15–25.

(20) Pietrobon, B.; McEachran, M.; Kitaev, V. Synthesis of Size-Controlled Faceted Pentagonal Silver Nanorods with Tunable Plasmonic Properties and Self-Assembly of These Nanorods. *ACS Nano* **2009**, *3*, 21–26.

(21) Hamon, C.; Novikov, S.; Scarabelli, L.; Basabe-Desmonts, L.; Liz-Marzán, L. M. Hierarchical Self-Assembly of Gold Nanoparticles into Patterned Plasmonic Nanostructures. *ACS Nano* **2014**, *8*, 10694–10703.

(22) Yang, Y.; Wang, W.; Li, X.; Chen, W.; Fan, N.; Zou, C.; Chen, X.; Xu, X.; Zhang, L.; Huang, S. Controlled Growth of Ag/Au Bimetallic Nanorods through Kinetics Control. *Chem. Mater.* **2013**, *25*, 34–41.

(23) Park, K.; Koerner, H.; Vaia, R. A. Depletion-Induced Shape and Size Selection of Gold Nanoparticles. *Nano Lett.* **2010**, *10*, 1433–1439.

(24) Agarwal, U.; Escobedo, F. A. Mesophase Behaviour of Polyhedral Particles. *Nat. Mater.* **2011**, *10*, 230–235.

(25) Damasceno, P. F.; Engel, M.; Glotzer, S. C. Predictive Self-Assembly of Polyhedra into Complex Structures. *Science* **2012**, *337*, 453–457.

(26) Boles, M. A.; Engel, M.; Talapin, D. V. Self-Assembly of Colloidal Nanocrystals: From Intricate Structures to Functional Materials. *Chem. Rev.* **2016**, *116*, 11220–11289.

(27) Zhou, S. et al. Chiral Assemblies of Pinwheel Superlattices on Substrates. *Nature* **2022**, *612*, 259–265.

(28) Wang, Z.; Schliehe, C.; Bian, K.; Dale, D.; Bassett, W. A.; Hanrath, T.; Klinke, C.; Weller, H. Correlating Superlattice Polymorphs to Internanoparticle Distance, Packing Density, and Surface Lattice in Assemblies of PbS Nanoparticles. *Nano Lett.* **2013**, *13*, 1303–1311.

(29) Quan, Z.; Xu, H.; Wang, C.; Wen, X.; Wang, Y.; Zhu, J.; Li, R.; Sheehan, C. J.; Wang, Z.; Smilgies, D.-M.; Luo, Z.; Fang, J. Solvent-Mediated Self-Assembly of Nanocube Superlattices. *J. Am. Chem. Soc.* **2014**, *136*, 1352–1359.

(30) Hamon, C.; Goldmann, C.; Constantin, D. Controlling the Symmetry of Supercrystals Formed by Plasmonic Core–Shell Nanorods with Tunable Cross-Section. *Nanoscale* **2018**, *10*, 18362–18369.

(31) Wei, W.; Wang, Y.; Ji, J.; Zuo, S.; Li, W.; Bai, F.; Fan, H. Fabrication of Large-Area Arrays of Vertically Aligned Gold Nanorods. *Nano Lett.* **2018**, *18*, 4467–4472.

(32) Wang, D.; Hermes, M.; Kotni, R.; Wu, Y.; Tasios, N.; Liu, Y.; de Nijs, B.; van der Wee, E. B.; Murray, C. B.; Dijkstra, M.; van Blaaderen, A. Interplay between Spherical Confinement and Particle Shape on the Self-Assembly of Rounded Cubes. *Nat. Commun.* **2018**, *9*, 2228.

(33) Zhao, K.; Mason, T. G. Twinning of Rhombic Colloidal Crystals. *J. Am. Chem. Soc.* **2012**, *134*, 18125–18131.

(34) Gong, J.; Newman, R. S.; Engel, M.; Zhao, M.; Bian, F.; Glotzer, S. C.; Tang, Z. Shape-Dependent Ordering of Gold Nanocrystals into Large-Scale Superlattices. *Nat. Commun.* **2017**, *8*, 14038.

(35) García-Lojo, D.; Modin, E.; Gómez-Graña, S.; Impéror-Clerc, M.; Chuvilin, A.; Pastoriza-Santos, I.; Pérez-Juste, J.; Constantin, D.; Hamon, C. Structure and Formation Kinetics of Millimeter-Size Single Domain Supercrystals. *Adv. Funct. Mater.* **2021**, *31*, 2101869.

(36) Quan, Z.; Fang, J. Superlattices with Non-Spherical Building Blocks. *Nano Today* **2010**, *5*, 390–411.

(37) Wang, C.; Dong, K.; Yu, A. Structural Characterization of the Packings of Granular Regular Polygons. *Phys. Rev. E* **2015**, *92*, 062203.

(38) Shen, W.; Antonaglia, J.; Anderson, J. A.; Engel, M.; Anders, G. v.; Glotzer, S. C. Symmetries in Hard Polygon Systems Determine Plastic Colloidal Crystal Mesophases in Two Dimensions. *Soft Matter* **2019**, *15*, 2571–2579.

(39) Cersonsky, R. K.; van Anders, G.; Dodd, P. M.; Glotzer, S. C. Relevance of Packing to Colloidal Self-Assembly. *Proc. Natl. Acad. Sci. U.S.A.* **2018**, *115*, 1439–1444.

TOC Graphic